phys. stat. sol. (a) **150**, 427 (1995)

Subject classification: 68.35; 61.14; S7.12; S7.15

*Max-Planck-Institut für Festkörperforschung, Stuttgart*[1]) *(a)*,
*IV. Physikalisches Institut der Universität Göttingen*[2]) *(b)*,
*Ferdinand-Braun-Institut für Höchstfrequenztechnik Berlin im Forschungsverbund Berlin e. V.*[3]) *(c)*,
*Bundesanstalt für Materialforschung und -prüfung, Berlin*[4]) *(d)*, *and*
*Max-Planck-Institut für Mikrostrukturphysik, Halle/Saale*[5]) *(e)*

# TEM Characterization of the Interface Quality of MOVPE Grown Strained InGaAs/GaAs Heterostructures

By

A. HÖPNER (a), H. SEITZ (b), I. RECHENBERG (c), F. BUGGE (c), M. PROCOP (d), K. SCHEERSCHMIDT (e), and H. J. QUEISSER (a)

*(Received May 16, 1995)*

Dedicated to Professor Dr. JOHANNES HEYDENREICH on the occasion of his 65th birthday

In order to optimize the growth conditions of strained-layer InGaAs QW high-performance lasers by MOVPE, different growth parameters are systematically varied. These test structures as well as complete laser structures are carefully analysed. Special attention is given among others to the homogeneity and interface quality of the quantum well. For "thicker" QW layers (>7 nm) – grown under standard conditions – it is possible to prove an increased smearing of the upper QW interface. This observation is in good correlation with AES measurements. For the first time, the inhomogeneous In distribution in the QW could be visualized as a detectable segregation of In in the interface region by using high-resolution TEM techniques and new methods of image analysis.

Zur Optimierung der Wachstumsbedingungen bei der Züchtung von „strained layer" InGaAs-QW-Hochleistungslasern mittels MOVPE werden die verschiedenen Wachstumsparameter systematisch variiert und die verschiedenen Teststrukturen sowie komplette Laserstrukturen einer umfassenden Analytik unterzogen. Besonderes Augenmerk gilt u. a. der Homogenität und Grenzflächenqualität des QW. In guter Korrelation zu AES-Messungen gelingt es bei „dickeren" QW-Schichten (>7 nm) – gezüchtet unter Standardbedingungen – eine deutlich verstärkte Verschmierung der oberen QW-Grenzfläche nachzuweisen. Erstmals kann die inhomogene In-Verteilung im QW, als nachweisbare Segregation des In im Bereich der Grenzflächen, mittels hochauflösender TEM-Techniken und neuartiger Bildauswerte-Verfahren sichtbar gemacht werden.

## 1. Introduction

Strained $In_xGa_{1-x}As/GaAs$ layers have attracted considerable attention owing to their application to microelectronic and optoelectronic devices. Especially the 0.98 μm InGaAs/GaAS/AlGaAs strained quantum well (QW) laser has attained a great interest due to its suitability for pumping erbium$^{3+}$-doped fiber amplifiers in fiber communication systems.

[1]) Heisenbergstr. 1, D-70569 Stuttgart, Federal Republic of Germany.
[2]) Bunsenstraße 13–15, D-37073 Göttingen, Federal Republic of Germany.
[3]) Rudower Chaussee 5, D-12489 Berlin, Federal Republic of Germany.
[4]) Unter den Eichen 87, D-12205 Berlin, Federal Republic of Germany.
[5]) Weinberg 2, D-06120 Halle, Federal Republic of Germany.

The performance of devices incorporating $In_xGa_{1-x}As$ strained layers was determined by the crystalline perfection and interface quality of the epitaxial layers. For the crystal growth of high perfection strained layers the critical thickness for the onset of the three-dimensional growth and lattice relaxation processes have to be taken into account as well as defect development after effects of In segregation [1 to 8]. After optimizing crystal growth parameters with regard to defect-free layers [9], we have investigated the influence of the deposition temperature, the growth interruption time at the upper $In_xGa_{1-x}As/GaAs$ interface, and the V/III ratio on the interface quality using transmission electron microscopy (TEM). We applied different TEM techniques, especially dark-field (DF) imaging and high-resolution transmission electron microscopy (HRTEM) [10 to 14] in combination with the well-known "chemical mapping" developed by Ourmazd et al. [15] and a new method of characterizing the tetragonal strain [16] to show the interface roughness and compositional variations in the strained layer. It is very difficult to distinguish between the morphological roughness and the compositional gradient at the interfaces, and it is generally impossible if both are of the same extention.

Furthermore, it is well-known that for the deposition of III/V material the segregation of indium under molecular beam epitaxy (MBE) conditions is a strong problem, which was investigated intensely as a function of deposition parameters [17 to 21]. On the other hand, the indium segregation under metal-organic vapor phase epitaxy (MOVPE) conditions has rarely been analysed [22, 23]. In our investigations, both laser structures and test structures are incorporated.

## 2. Experimental Procedure

The MOVPE growth was performed in a horizontal reactor at a total pressure of hPa. Starting materials were pure arsenic, trimethyl aluminium, gallium, and indium. Dimethyl zinc was used for p-type doping, diselane diluted in hydrogen for n-type doping. Separate confinement heterostructure (SCH) lasers were prepared on (100) n-type GaAs substrates.

The structure of the sample of type A is shown in Fig. 1, consisting of $In_xGa_{1-x}As$ QW ($x_{nom} = 0.24$) sandwiched between GaAs spacer layers and $Al_yGa_{1-y}As$ confinement and cladding layers. Samples of type B possesse a double QW (DQW), 15 nm thick GaAs spacer layers, graded $Al_{0.24}Ga_{0.76}As$ (500 nm thick)/$Al_{0.29}/Ga_{0.71}As$ (1000 nm thick). The critical thickness for lattice relaxation processes is much higher than the thickness of all QW layers in this investigation. The doping concentrations were $1 \times 10^{17}$ cm$^{-3}$ for confinement layers and $1 \times 10^{18}$ cm$^{-3}$ for cladding layers [24, 25].

For TEM investigations most of the samples were prepared as ⟨110⟩ and ⟨100⟩ cross sections. After the mechanical preparation focused ion beam thinning was used to prepare TEM transparent regions of the whole layer structure. In this way, it was possible to determine the precise layer thickness. The In content of each sample was determined by photoluminescence (PL). JEOL 2000 FX and 4000 FX microscopes (both instruments with EDX systems) were applied for diffraction contrast, lattice fringe and ⟨110⟩ HRTEM imaging, whereas for ⟨100⟩ HRTEM imaging a Philips CM 30/ST and the JEOl 4000 EX operating at 300 and 400 kV, respectively, were used.

The tetragonal strain was detected and quantified by analysing HRTEM lattice images using the strain mapping method. This could be achieved by determining intensity maxima within the image dots of the lattice images. The evaluation of the distances between the intensity maxima reveals the amount of tetragonal distortions of the atomic positions of

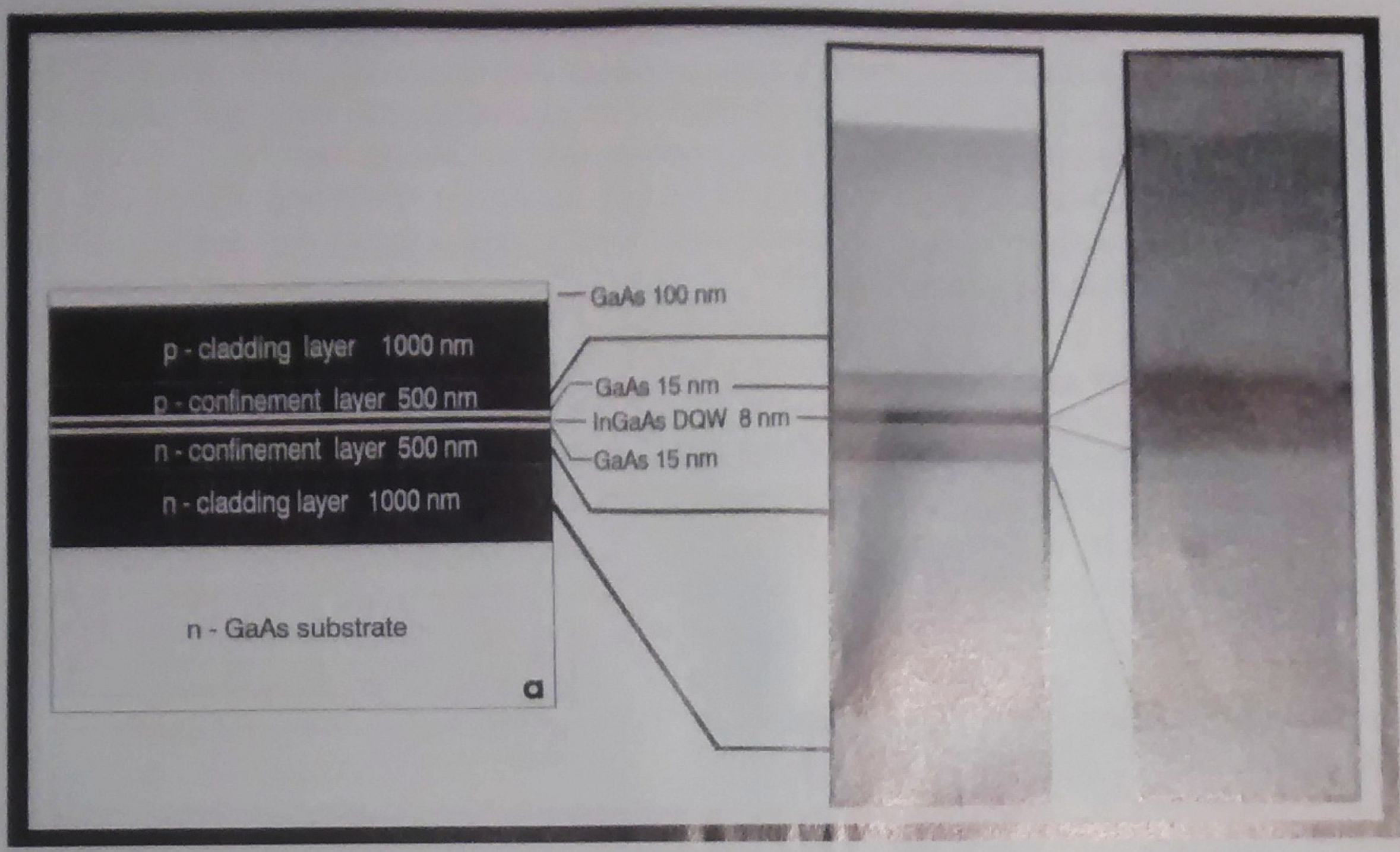


Fig. 1. a) Scheme of the separate confinement heterostructure (SCH) laser diode, b) HR image of the active zone, and c) [200] lattice fringe image of the QW region

the specimen. The net grid of the image unit cells is produced by connecting the intensity maxima by the strain mapping method. The differences between the intensity maxima produce image unit cells of different size between each other and a net grid adjusted to the local image structure. The size of the image unit cell determines the spatial resolution, which can be decreased down to near-atomic values (see, e.g., Fig. 7b). The detection limit of tetragonal strains is determined by the amount of noise in the image, depending on the number of intensity maxima within the unit cell and therefore on the size of the unit cell. The method is described in detail in [16]. Here the strain mapping has been smoothed to obtain a better qualitative analysis lowering the spatial resolution. The most important problem of the strain mapping method consists in finding a sufficiently clear relation between tetragonal strains measured from the images and the strains existing in the object. This will be discussed by comparing strain curves measured by a very similar method but using the atomic coordinates of structure models for the image simulations (see Fig. 7 and 8). The detailed analysis of the strains known from a model and compared with those measured in the simulated images will be given elsewhere.

The strain mapping method can be combined with chemical lattice imaging (detailed description in [15]). Imaging conditions suitable for chemical lattice imaging have to be chosen to yield a linear relation between the in-plane angle and the differences in the chemical composition. After the templates are selected the vector pattern recognition calculates the in-plane angle, which is the measurement of the relative variation of the patterns of each image unit cell. The values of the in-plane angles range between the values of the patterns of the two templates.

In addition to the TEM investigations, the In concentration profile was monitored by Auger electron spectroscopic (AES) depth profiling. Structures like that of type A, but without the $Al_yGa_{1-y}As$ layers were profiled. The measurements were performed at a Scanning Auger Microprobe PHI 595. The primary electron energy was 5 keV. To achieve a good depth resolution a low ion energy of 0.6 keV for Ar ion sputtering was chosen. For the same reason Auger lines with low escape depths were selected for depth profiling: Ga(MMM), As(MMM), and In(MNN).

## 3. Results and Discussion

In Table 1, the structural quality of the QWs characterized by TEM (the low defect density was verified by cathodoluminescence (CL)) is correlated with the growth parameters. We have varied the growth temperature ($T_{growth}$), the differential reactor pressure (V/III ratio), and the time of growth interruption between the upper InGaAs QW and the GaAs spacer layer. The effects of growth interruption were measured also by PL and CL, in which the 10 K spectrum shows a very broad peak for samples without growth interruption. The results suggest optimum growth for a growth interruption of 10 to 20 s [24].

Table 1
Variation of growth parameters and results of TEM investigations

| sample Nr. | sample Nr. of growth | growth parameters | | | | TEM | | | |
|---|---|---|---|---|---|---|---|---|---|
| | | sample structure | $T_{growth}$ (°C) | V/III ratio | $t_{IF\text{-}interrupt}$ (s) | $d_{QW}$ (nm) | $r_{defect}$ ($cm^2$) | interface-quality lower QW IF | interface-quality upper QW IF |
| T1 | 2773 | TestPL | 750 | 150 | 10 | >7 | $\approx 10^7$ | >4 | >4 |
| T2 | 2903 | Test[a]) | 700 | 150 | 10 | 5.1 | $\approx 10^{7\text{ to }8}$ | 3 | >4 |
| A1 | 2863 | c. laser[b]) | 750 | 150 | 10 | 5.6–7.0 | $<10^{2}$[f]) | 2 | 3–4 |
| A2 | 020055 | c. laser | 750 | 150 | 10 | 6.5–7.9 | $\approx 10^{4}$[f]) | 2 | 3 |
| A3 | 020056 | c. laser | 750 | 150 | 10 | 5.9– | $<10^{3}$[f]) | 3 | $\approx 10$ |
| A4 | 020097 | c. laser | 750 | 150 | 5 | 5.6–6.7 | $<10^{3}$[f]) | 2 | 3 |
| A5 | 020099 | c. laser | 750 | 150 | 20 | 6.2–7.6 | $<10^{3}$[f]) | 2 | 3 |
| A6 | 020117 | c. laser | 750 | 150 | 10 | 5.1–6.0 | – | 1–2 | 2–3 |
| A7 | 020118 | c. laser | 650 | 150 | 10 | 6.8–7.3 | – | 1–2 | 1–2 |
| T3 | 9312 | TestAES1[c]) | 750 | 150 | 10 | 7 | | 2 | >10 |
| B | 020200 | DQW[d]) | 750 | 150 | 10 | 6.7–8.4 | | 2 | 5–7 |
| T4 | 020224 | TestTEM1[e]) | 750 | 25/75/ 150/300 | 5/20/40 | 5.6–7.0 | | 2 | 4 |
| T5 | 020225 | TestTEM2[e]) | 650 | 25/75/ 150/300 | 5/20/40 | 6.2–6.8 | – | 2–3 | 2–3 |
| | | | | | | 6.2–6.5 | – | 1–2 | 1–2 |

[a]) One of the first MOCVD test structures.
[b]) One of the best complete laser structures before the equipment was reconstructed.
[c]) Special test structures to measure the In distribution by AES.
[d]) Double quantum structure for PL investigations.
[e]) Test structure to check the influence of growth parameters by TEM methods.
[f]) Determined by cathodoluminescence.


Fig. 2. Electron diffraction contrast image showing high densi

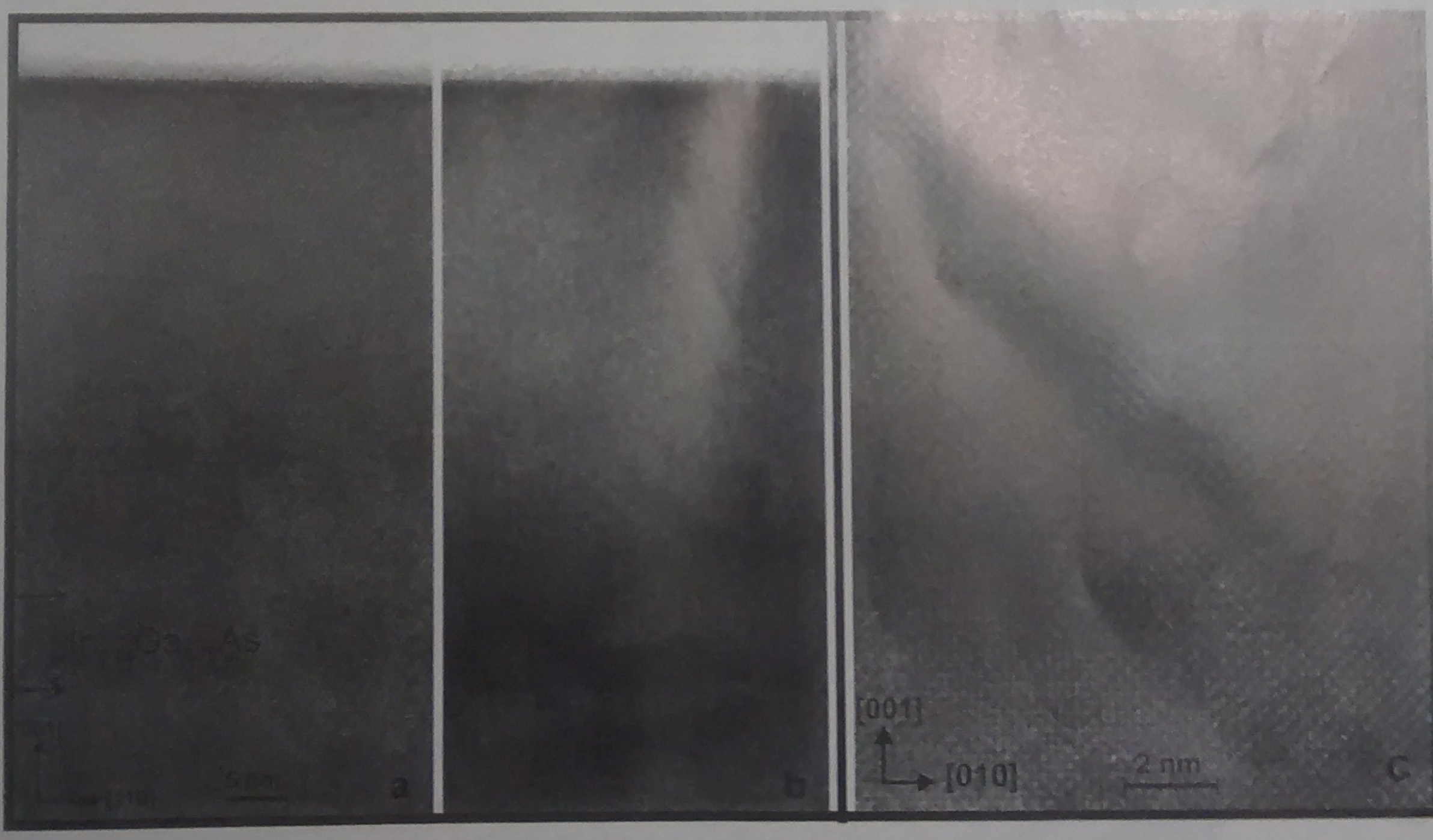


Fig. 3. HRTEM images of the AES test structure T3 in different cross section orientations sho
a) the smeared upper interface of the QW, b) superimposed diffraction contrast around disturbed regio
caused by strains, and c) the ⟨100⟩ phase contrast of disturbed regions

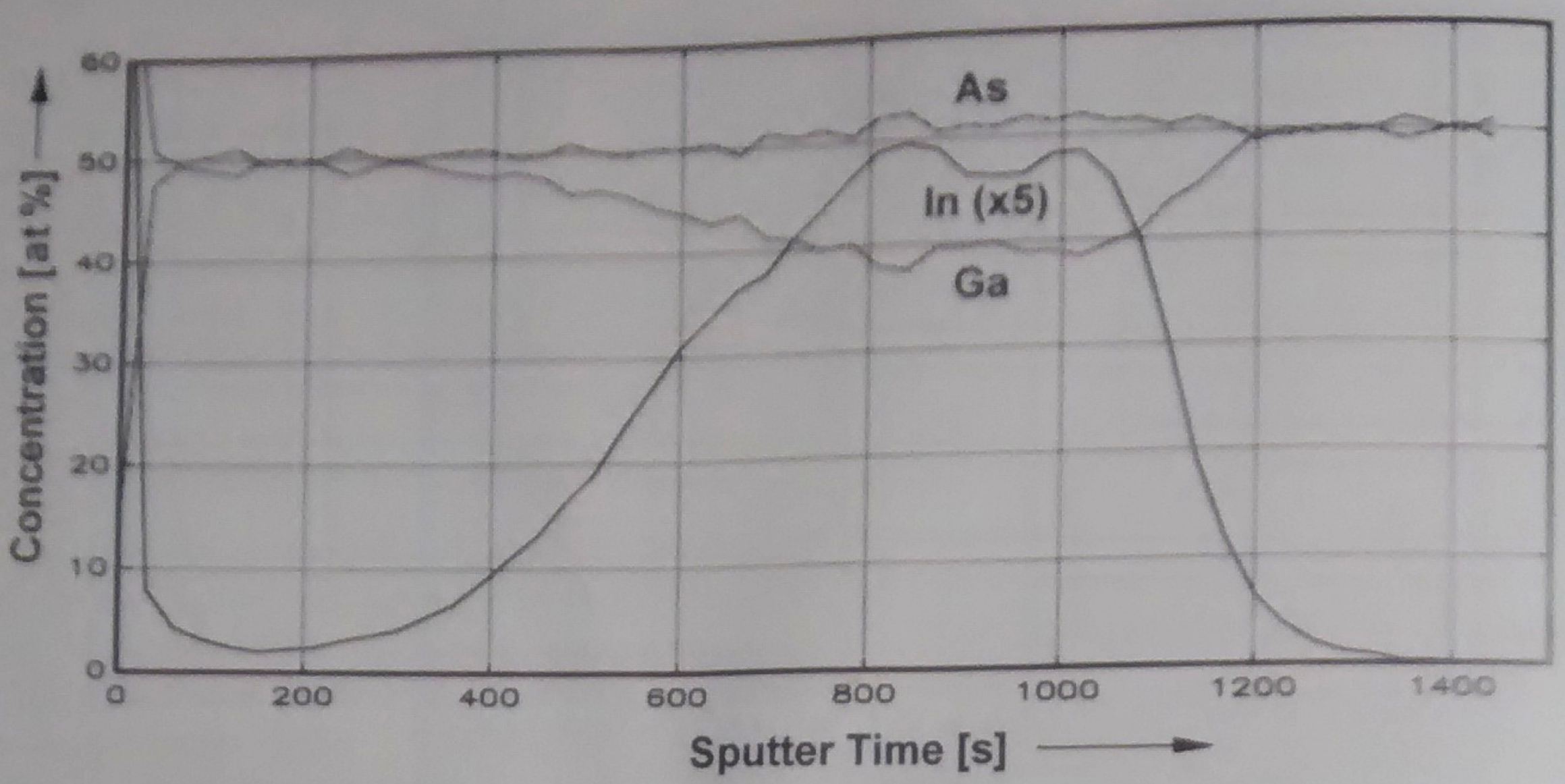


Fig. 4. AES depth profile of the layer structure of sample T3

At the beginning of our investigations of MOVPE laser structures there was a very high density of structural defects (see Fig. 2), in particular, threading dislocations and small strained and disturbed regions in the $In_xGa_{1-x}As$-QW ($x \approx 0.3$).

An obvious reduction of defects was achieved by slightly reducing the In content, which was now 24%. In order to provide the same emission wavelength as that of the samples with not reduced In content thicker QW layers were grown. Under growth conditions (temperature, total pressure) otherwise not modified these layers showed a lower defect density (especially dislocation density). A "smearing out" of the upper QW interface clearly manifested itself. By the superposition of the phase contrast with the diffraction contrast the images of sample T3 in Fig. 3a, b clearly indicate the difference in the extension of the

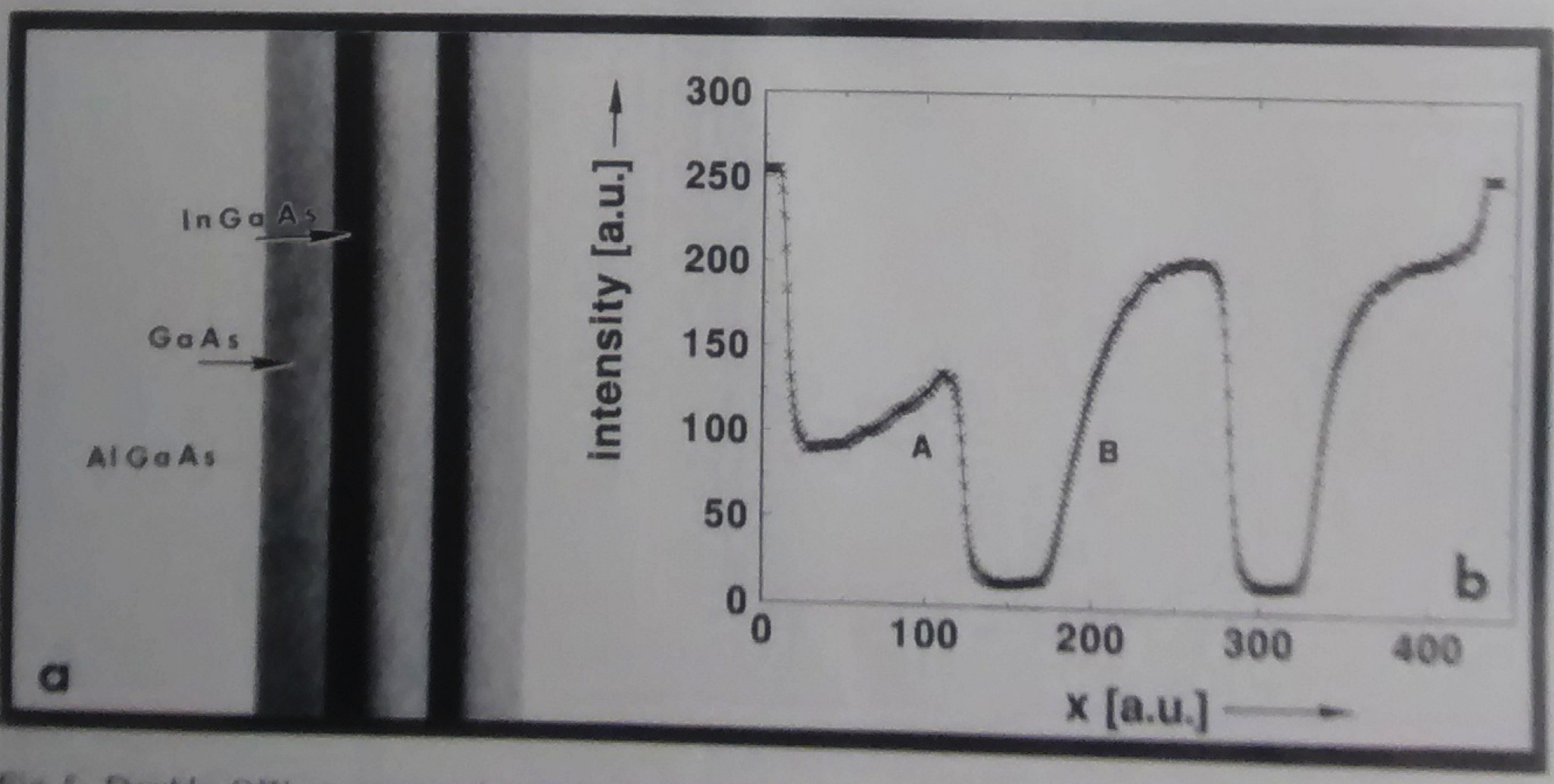


Fig. 5. Double QW structure of sample B in a) the (200) DF image and b) the averaged intensity profile (intensity and $x$ in arbitrary units)

upper and the lower QW interface, similarly to corresponding DF images. Fig. 3b and c show the distorted regions in ⟨110⟩ and ⟨100⟩ projection. EDX analysis revealed an In concentration locally increased on these spots.

The asymmetric AES depth profile of sample T3 (Fig. 4), shows a slight decrease of the In concentration to the surface of the GaAs surface layer. The In was segregated at the QW interfaces and incorporated by almost the entire 30 nm GaAs layer. At the surface it had finally segregated. The In concentration at the centre of the QW was determined to be $x = 0.18 \pm 0.01$.

A similar behaviour was also oberserved of the double QW structures (sample type B) by TEM (Fig. 5). The surface-oriented interface, marked by "B", of the thicker QW in Fig. 5b exhibits also a marked smearing in the cross-sectional profile of about 100 nm. This cross-sectional profile was averaged over several thousand measuring points.

In order to recognize possible sources of degradation of laser diodes, different testing structures were investigated. Two structures with seven $In_{0.18}Ga_{0.82}As$ QWs were especially grown under different growth conditions for investigating the interface roughness in HRTEM. Due to their $Al_{0.3}Ga_{0.7}As$ interlayers, it was possible to image these structures in a very good layer contrast. Fig. 6a shows the layer, which was grown at a pressure ratio of 150, for a growth interruption of 10 s on the upper interface and at a temperature of 650 °C. This layer represents one of the layers having the best upper interface. A more detailed characterization of the interface roughness by means and strain mapping showed a sharp interface (transition independently of the image unit cell employed (see Fig. 6b). However, of 650 °C, there was a marked vertical distortion in both especially for strain mapping. This distortion can be interpreted of the In content at the interfaces of the QW. In Fig. an inhomogeneous In distribution.

On the basis of the expected far less pronounced layers and the InGaAs QW respectice simulations show the influence of various In distributions on the HRTEM contrast. A more visual characterization of the interface quality of complete laser structures without AlGaAs interlayers is hardly possible. For this purpose, both a model of the active region of the complete laser structure for various imaging conditions was simulated (see Fig. 7 and 8) as well as a variety of differently graded (gradual) interface transition regions. With the help of the CERIUS program package, supercell models, consisting of different layers of InGaAs/AlGaAs/GaAs were generated by the stoichiometric replacement of Ga by In and Al atoms, respectively, with a subsequent relaxation of the structure using molecular dynamics (MD). The generation and relaxation of the structures as well as the HRTEM image simulations on the basis of such relaxed structures are described in [26]. Fig. 7d shows one of the models of a laser structure used for the HRTEM image simulations (Fig. 8a, b) and the strain measurement (Fig. 8c). Fig. 8a, b demonstrate a defocus series ($\Delta$ in nm) for thickness $t = 13.5$ nm of an unrelaxed (Fig. 8a) structure and a relaxed one (Fig. 8b). The strain measurement (Fig. 8c) demonstrates the dependence of the strains on the location in the model: the lattice distance variations differ with the position of the net grid.

The inhomogeneous In distribution of the QW profile is clearly displayed in the ⟨100⟩ HRTEM images processed by chemical mapping (Fig. 7b) and strain mapping (Fig. 7c). These structures are characterized by a strong In enrichment at the lower very smooth

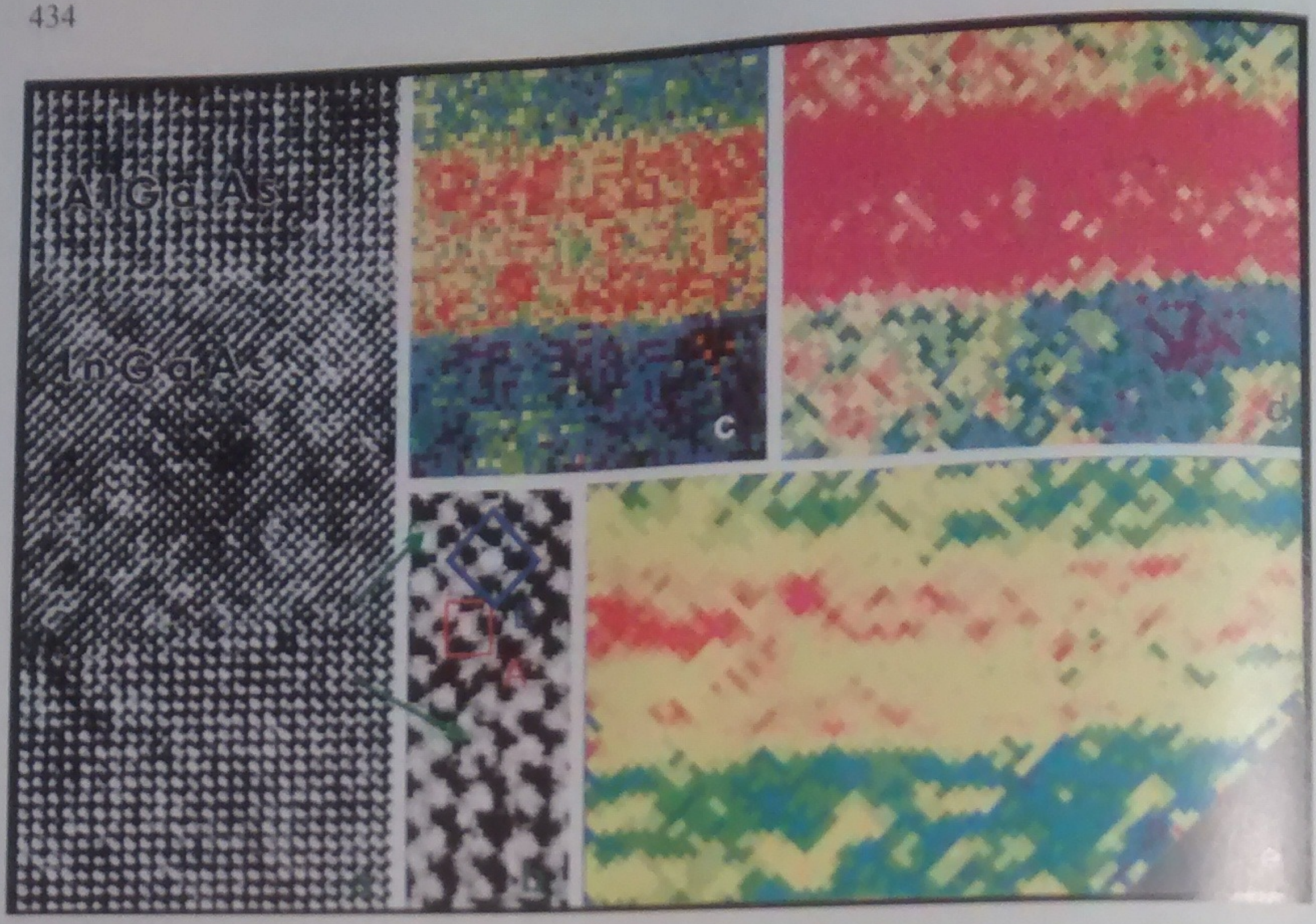


Fig. 6. a) ⟨100⟩ HRTEM image of test structure T5 with the lower interface partly enlarged (b) showing the two different image unit cells "A" and "B", which are used for chemical mapping ("A" in Fig. 6c and "B" in Fig. 6d). c) The strain mapping with image unit cells of type B

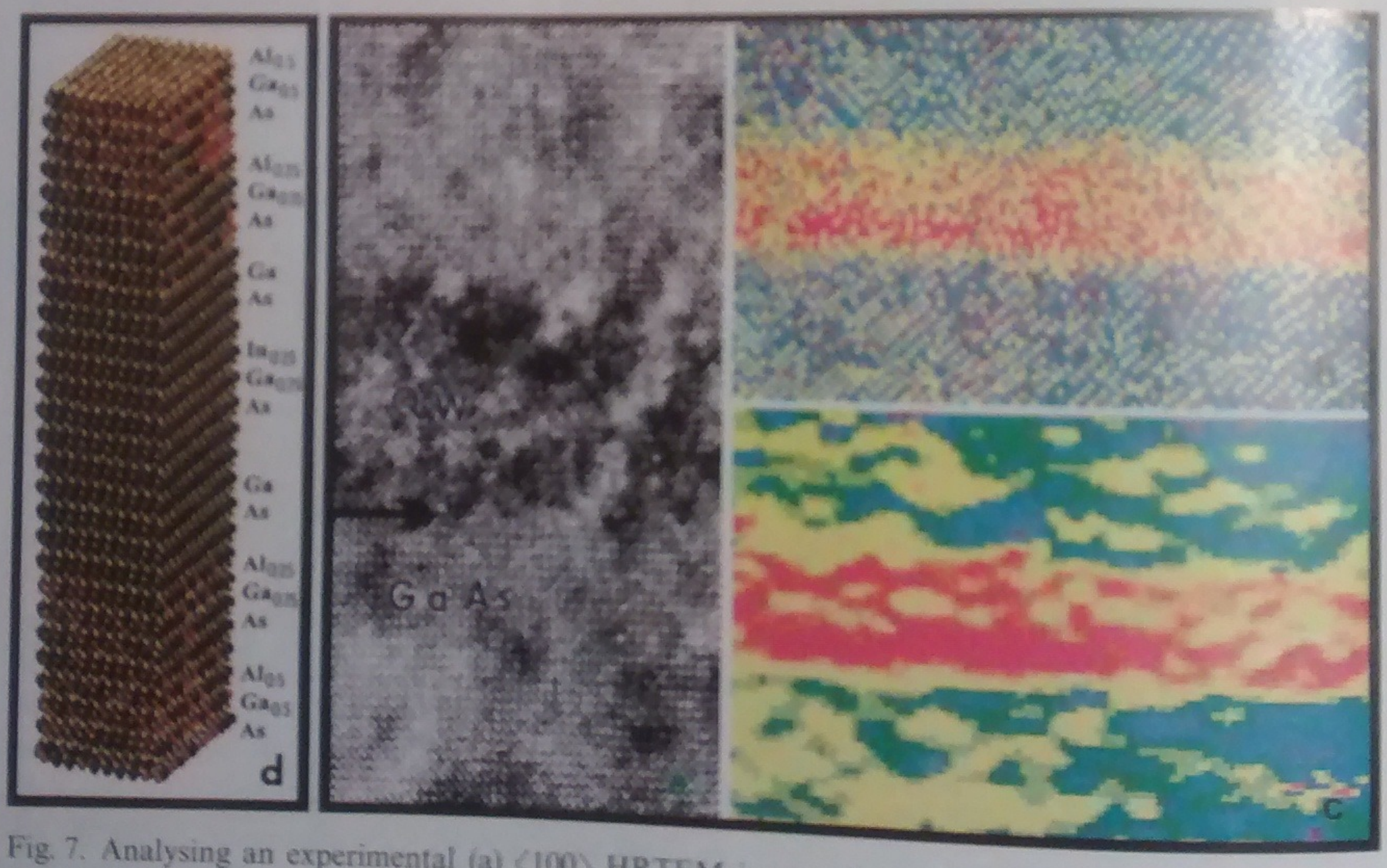


Fig. 7. Analysing an experimental (a) ⟨100⟩ HRTEM image of the QW region of sample A1 by b) chemical mapping and c) strain mapping using small size unit cells of type "A". d) Model of an AlGaAs/GaAs/InGaAs QW structure relaxed by MD

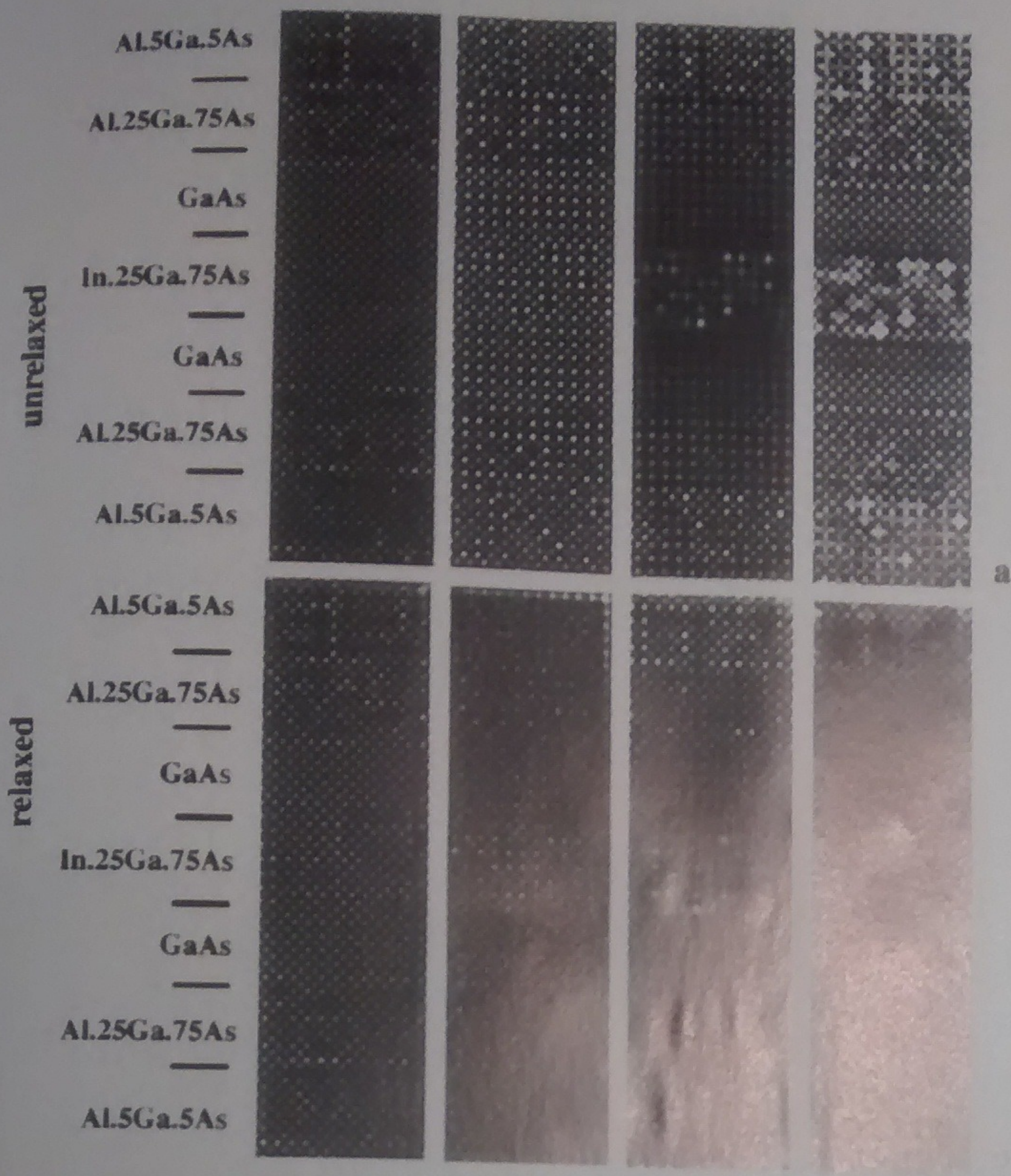


Fig. 8. HRTEM image simulations for an AlGaAs/GaAs/InGaAs QW structure: a) unrelaxed and b) relaxed by molecular dynamics for different defoci ($\Delta$ in nm, $U = 400$ kV, $C_s = 1$ mm, $\alpha = 1.6$ nm$^{-1}$, $\delta = 8$ nm, $\alpha_d = 0.5$ mrad, $t = 13.5$ nm) as well as c) strains measured across the QW at the centre of the model (i), near the exit face (ii), and a side face (iii)

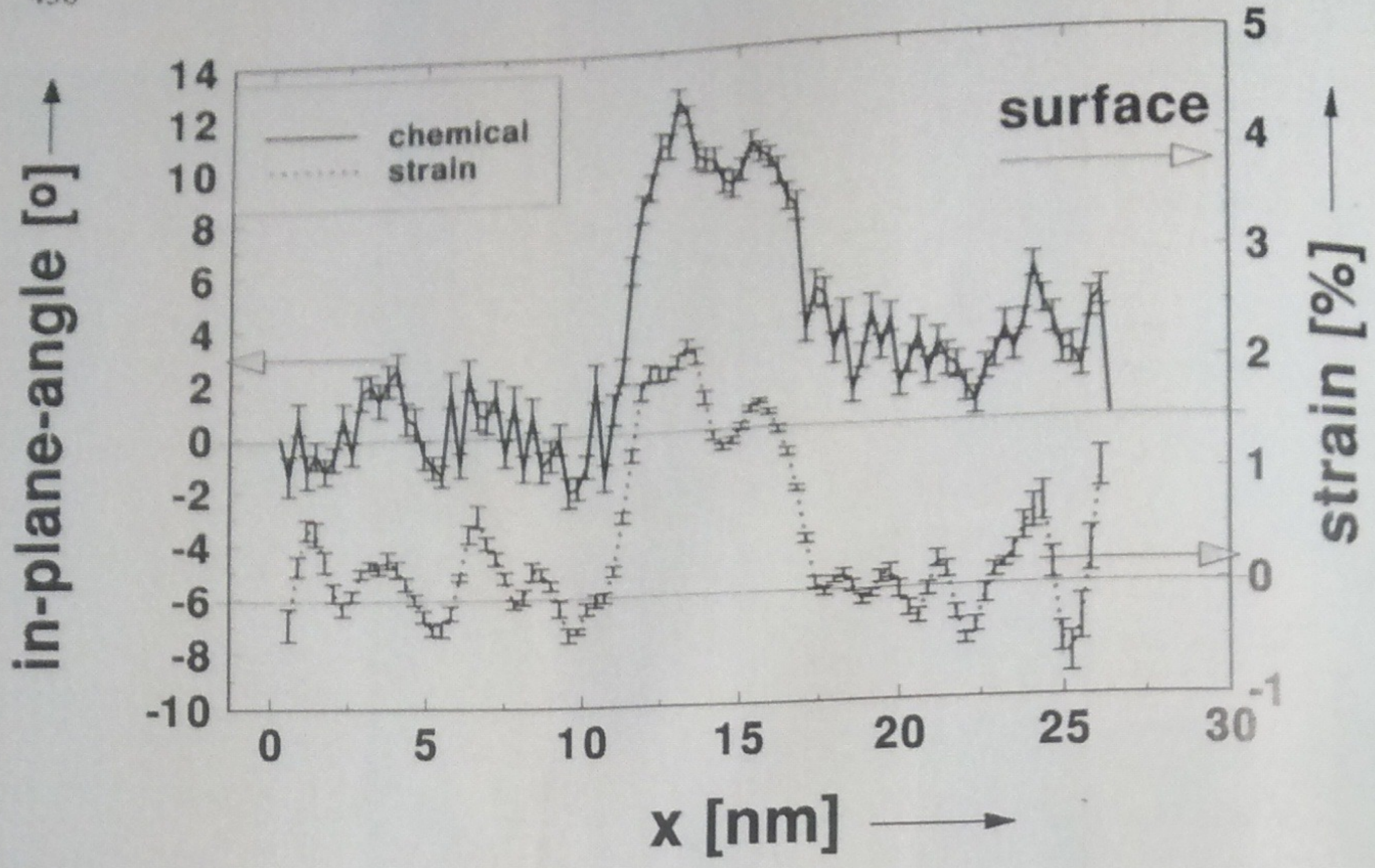


Fig. 9. Averaged chemical mapping and strain mapping profiles of Fig. 7b, c

QW interface and by an In accumulation smeared over four monolayers at the upper interface. The averaged profiles of the active zone of the laser structure (Fig. 7b, c) are shown in Fig. 9.

## 4. Conclusions

MOVPE InGaAs QW structures grown at 750 °C differ from those grown by MBE at significantly lower temperatures. They tend to precipitate In and to form defects at much lower In concentrations than samples grown by MBE. This tendency seems to be due to the generally higher growth temperatures. At temperatures of 650 °C there was no precipitation. Based on the good agreement of TEM and AES investigations it was possible to prove an inhomogeneous smearing over several nm out of the upper interface of samples of an In content close to the In precipitation limit. If the In content is further reduced, at a growth temperature of 750 °C the upper interface transition area is reduced from over ten monolayers to three or four monolayers. With about 2 ML the lower QW interface turns out to be sharp and absolutely smooth over large areas. Reducing the growth temperature to 650 °C (under standard conditions) finally resulted in transition widths of 1 to 2 ML of the upper interface.

All samples, even those grown at lower growth temperatures, had an In concentration profile in the QW which clearly pointed out an In segregation at the QW interfaces.

*Acknowledgements*

The authors are very thankful to A. Klein and I. Purann for preparing numerous TEM cross section samples. Thanks are also due to Prof. Dr. M. Rühle and Dr. R. Ramlau for the permission to use their electron microscopes. The work was supported by the Deutsche Forschungsgemeinschaft contract Re 954/1 – 4.

## References


[1] J. Y. Yao, T. G. Andersson, and G. L. Dunlop, J. appl. Phys. **69**, 2224 (1991).
[2] E. A. Fitzgerald, D. G. Ast, P. D. Kirchner, G. D. Petti, and J. M. Woodall, J. appl. Phys. **63**, 693 (1988).
[3] S. Guha, K. C. Rajkumar, and A. Madhukar, J. Crystal Growth **111**, 434 (1991).
[4] J.-P. Reithmaier, H. Richert, and H. Schlötterer, J. Crystal Growth **111**, 407 (1991).
[5] K. H. Chang, P. K. Bhattacharya, and R. Gibala, J. appl. Phys. **66**, 2993 (1993).
[6] M. Tamura, A. Hashimoto, and Y. Nakatsugawa, Mater. Res. Soc. Symp. Proc. **295**, 123 (1992).
[7] J. Wang, J. W. Steeds, and D. A. Woolf, Phil. Mag. **65**, 829 (1992).
[8] C. Shouzen, T. Chang, and L. Sichen, J. appl. Phys. **73**, 4916 (1993).
[9] I. Rechenberg, F. Bugge, A. Höpner, A. Klein, and U. Richter, Inst. Phys. Conf. Ser. **135**, 327 (1994).
[10] H. Cerva, Appl. Surface Sci. **50**, 19 (1991).
[11] W. M. Stobbs and W. O. Saxton, J. Microscopy **151**, 171 (1988).
[12] W. M. Stobbs, C. S. Baxter, E. G. Bithell, C. B. Boothroyd, R. F. Broom, F. M. Ross, and E. J. Williams, Inst. Phys. Conf. Ser. **100**, 271 (1989).
[13] A. Höpner, K. Köhler, D. J. As, and M. Maier, Proc. 10th Europ. Congr. EM, Vol. 2, 1992 (p. 129).
[14] M. Maier, K. Köhler, A. Höpner, and D. J. As, J. appl. Phys. 73, 3820 (1993).
[15] A. Ourmazd, F. H. Baumann, M. Bode, and Y. Kim, Ultramicroscopy **34**, 327 (1990).
[16] H. Seitz, F. H. Baumann, M. Seibt, K. Ahlborn, and W. Schröter, phys. stat. sol. (a) **150**, No. 2 (1995).
[17] J. M. Moison, C. Guille, F. Houzay, F. Barthe, and Van Rompay, Phys. Rev. B **40**, 6149 (1989).
[18] J. M. Moison, F. Houzay, F. Barthe, J. M. Gérald, and B. Jusserand, J. Crystal Growth **111**, 141 (1991).
[19] J. Nagle, J. P. Landesmann, M. Larive, C. Mottet, and P. Bois, J. Crystal Growth **127**, 495 (1993).
[20] O. Brandt, L. Tapfer, K. Ploog, R. Bierwolf, and M. Hohenstein, Appl. Phys. Letters **61**, 2814 (1992).
[21] H. Toyoshima, T. Niwa, J. Yamazaki, and A. Okamoto, Appl. Phys. Letters **63**, 821 (1993).
[22] S. Lutgen, T. Marschner, W. Stolz, and E. O. Göbel, J. Crystal Growth (1995), in press.
[23] C. Frigeri, A. Di Paola, N. Gambacorti, D. M. Richie, F. Longo, and M. Della Giovanna, Mat. Sci. Engng. B **28**, 346 (1994).
[24] F. Bugge, G. Beister, G. Erbert, S. Gramlich, I. Rechenberg, H. Treptow, and M. Weyers, J. Crystal Growth **145**, 907 (1994).
[25] I. Rechenberg, A. Höpner, J. Maege, A. Klein, G. Beister, and M. Weyers, Inst. Phys. Conf. Ser., to be published.
[26] K. Scheerschmidt, S. Ruvimov, P. Werner, A. Höpner, and J. Heydenreich, J. Microscopy **179** (1995), in print.